RESEARCH ARTICLE

WILEY

Vulnerability assessment of peatland complexes in the Hudson Plains (Ontario, Canada) to permafrost-thaw-induced landcover and hydrological change using a multiscale approach

Mikhail Mack[1] [iD] | William Quinton[1] | James McLaughlin[2] | Christopher Hopkinson[3]

[1]Cold Regions Research Centre, Wilfrid Laurier University, Waterloo, Ontario, Canada

[2]Ontario Forestry Research Institute, Ontario Ministry of Natural Resources and Forestry, Sault Ste. Marie, Ontario, Canada

[3]Department of Geography and Environment, University of Lethbridge, Lethbridge, Alberta, Canada

Correspondence
Mikhail Mack, Cold Regions Research Centre, Wilfrid Laurier University, Waterloo, Ontario N2L 3C5, Canada.
Email: mackmikhail@gmail.com

Abstract

The Hudson Plains, Canada, is one of the largest, undisturbed peatland regions (370,000 km^2) in the world. Air temperature in the Hudson Plains is increasing rapidly leading to unprecedented permafrost thaw. The region's remoteness has hindered our knowledge of how permafrost thaw alters peatland land cover and hydrological response at multiple scales. To assess which landscapes in the Hudson Plains are vulnerable to such disturbances, we analysed latitudinal distributions of land cover over a 300-km transect spanning the sporadic (<30% areal) to continuous (>80% areal) permafrost zone in northern Ontario and quantified land cover changes over 40 years using multiple remote sensing datasets (lidar, air photographs, and high-resolution satellite imagery). We then evaluated these landscapes at a fundamental hydrological unit, the peatland complex, identified five peatland complex types, and conceptualized their potential hydrological response using circuitry analogues. Over four decades, we found that permafrost peatlands declined by 4%, 8.5%, and 2% areal in the sporadic, discontinuous, and continuous permafrost zones, respectively. Circuitry analogues partitioned peatland complexes into their component peatland forms (e.g., permafrost peatland, bog, and fen) and represented each component's hydrological function using an electrical equivalent (e.g., generator, switch, and conductor). When interpreted at the landscape scale, circuitry analogues demonstrated latitudinal patterns in landscape structure (i.e., circuitry wiring) and indicated where permafrost thaw will have the greatest impact on landscape structure (i.e., rewiring) and therefore hydrological response. Based on these analyses, we suggest a 60-km latitudinal segment (54.5°N to 54.9°N) where peatland complexes are most vulnerable to permafrost-thaw-induced land cover and hydrological change and should therefore be the focus of future research and monitoring efforts.

KEYWORDS
circuitry analogue, Hudson Plains, peatland complexes, permafrost peatlands

1 | INTRODUCTION

The 370,000-km^2 Hudson Plains ecozone in north-central Canada is the world's second-largest permafrost-affected peatland region (Figure 1). This ecozone extends from continental boreal environments in permafrost-free terrain to low-arctic tundra underlain by continuous permafrost (>80% areal) along the south-western Hudson Bay coast (Harris et al., 1988). Between these southern and northern limits lies an expansive peatland-dominated region of sporadic (<30% areal) and discontinuous (>30% to <80% areal) permafrost, with relatively minor occurrences of mineral wetlands, deeper waterbodies (>2 m deep), upland forests, and barren lands (Riley, 2011). Peatlands consist of two predominant wetland classes, bogs and fens (National Wetlands Working Group [NWWG], 1988). The primary source of water to bogs is precipitation, whereas, for fens, precipitation is augmented by surface and or subsurface inputs (NWWG, 1988). The large assemblages of bogs and fens in the Hudson Plains are typically arranged into peatland complexes (Cajander, 1913), with each multi-square kilometre complex containing its own internal topographical, hydrological, and ecological gradients.

With increasing latitude, peatland complexes in the Hudson Plains are increasingly composed of nonwetland peatland forms underlain by permafrost (Riley, 2011). Such 'permafrost peatlands' include polygonal peat plateaus, peat plateaus, palsas, and inter-ridge bogs/fens (Riley, 2011; Sjörs, 1959; Zoltai & Tarnocai, 1974), which typically rise 1–2 m above adjacent permafrost-free terrain. Detailed descriptions of permafrost-free and permafrost peatlands are found in the Supporting Information (Table S1). As permafrost peatlands thaw, these features transform into permafrost-free peatlands because of the simultaneous processes of ground surface subsidence and inundation. This transformation changes the flux and storage of water within and from the transformed peatland as preferential flow is no longer impeded by permafrost barriers. To address the question of the impact of climate warming on basin run-off in the Hudson Plains, a reasonable first step is to investigate the region's distribution of peatland complexes and how permafrost thaw is changing their component peatland forms and therefore hydrological function.

Little is known of the present distribution of permafrost peatlands in the Hudson Plains, how the distribution of these features changes with increasing latitude (e.g., McLaughlin & Webster, 2014; Riley, 2011), and how their presence and distributions have changed over recent decades (e.g., Kirkwood et al., 2019; Ou et al., 2016; Pironkova, 2017). Even less is known of how permafrost thaw affects the form and hydrological function of the peatland complexes of which they are a part. This is a significant dearth of knowledge considering that the Hudson Plains occupies the southernmost extent of nonalpine permafrost (Brown et al., 2002) and is therefore highly vulnerable to hydrological change resulting from permafrost thaw (Spence et al., 2020).

Several decades of field (Connon et al., 2014, 2015; Hayashi et al., 2004; Quinton et al., 2003), remote sensing (Carpino et al., 2018, 2021; Chasmer et al., 2014; Chasmer & Hopkinson, 2017), and numerical modelling (Devoie et al., 2019; Devoie & Craig, 2020) studies in the southern Taiga Plains ecozone of north-western Canada have characterized specific permafrost thaw processes, defined their rate and pattern, and characterized their effect on the form and hydrological function of the peatland complexes in permafrost terrain. Permafrost thaw reduces the ability of
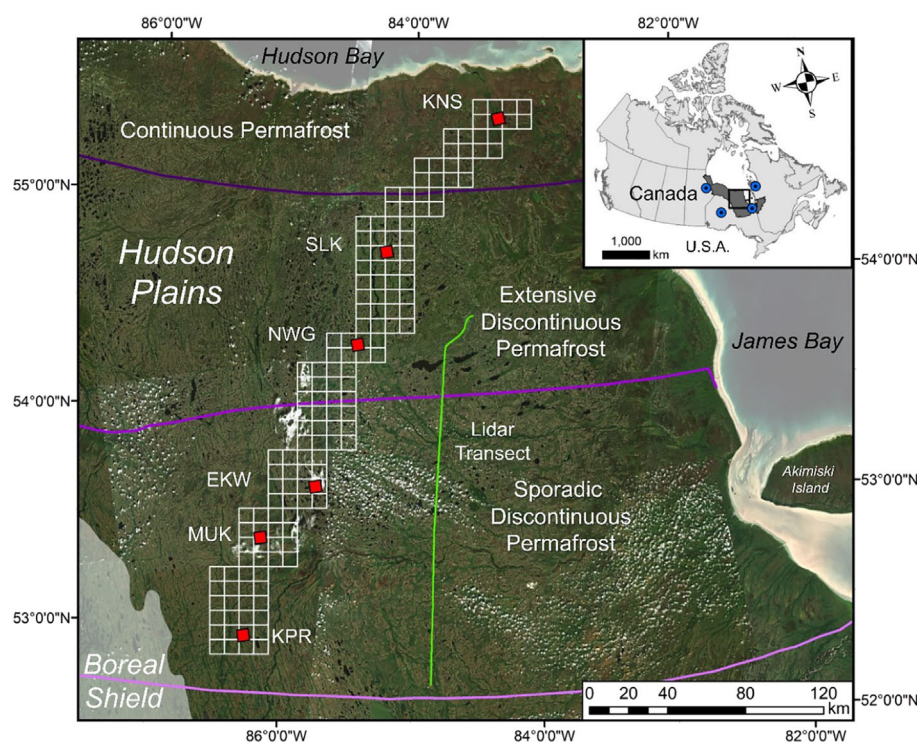

FIGURE 1 Map depicting the Hudson Plains study region, permafrost zonation, and transect locations. The lidar transect is shown in green and the gridded transect is shown in grey. Shown in red are the six 36-km2 areas of interest (AOIs). From south to north, AOI labels refer to Koper Creek (KPR), Muketei River (MUK), Ekwan River (EKW), North Washagami River (NWG), Sutton Lake (SLK), and Kinusheo River (KNS). The base map is a 'true colour' composite Sentinel-2A mosaicked image. Permafrost zonation is based on Brown et al. (2002) *Circum-Arctic Map of Permafrost and Ground-Ice Conditions*, Version 2. The subset map depicts the entire Hudson Plains domain (dark grey) within Canada and the nearest climate stations (blue dots) to our study area with 1981–2010 averages. From bottom left to bottom right in a clockwise direction, those climate stations are Pickle Lake, Gillam, Kuujjuarapik, and Moosonee.

the landscape to obstruct drainage and impound water (Connon et al., 2014; Hayashi et al., 2004; Quinton et al., 2003) and introduces new surface (Connon et al., 2015) and subsurface (Connon et al., 2018; Devoie et al., 2019) flow paths. As such, permafrost thaw increases the hydrological connectivity of peatland complexes (Connon et al., 2015), increases the hydrological response of streams (Connon et al., 2014; St. Jacques & Sauchyn, 2009), and partially drains areas of the landscape previously impounded by 'permafrost dams' (Haynes et al., 2018). However, a study by Mack et al. (2021) demonstrated that between 1970 and 2016, increased hydrological response was largely not seen in a cohort of peatland-dominated basins found in the sporadic and discontinuous permafrost zones outside the Taiga Plains, including four basins in the Hudson Plains. Regionally slower permafrost thaw rates and more diverse land cover assemblages were possible explanations for the absence of any change. The knowledge gained from these studies provides valuable and detailed information directly applicable to the interpretation of changes to landscapes in the Hudson Plains observed through remote sensing.

The few remote sensing observations (e.g., Kirkwood et al., 2019; Ou et al., 2016; Pironkova, 2017) suggest that permafrost thaw is changing peatland forms throughout the Hudson Plains, and as a result, the region is potentially in a state of ecohydrological transition without precedent in the historical record. Aerial and/or satellite images provide snapshots of the spatial arrangement of peatlands and peatland complexes, and the comparison of images representing different times can therefore show permafrost thaw-induced changes to peatland forms and hydrological function.

As permafrost thaw changes the relative proportion of permafrost peatland forms and therefore the composition of peatland complexes, the flux and storage of water within and from such complexes must also change. In this study, we examine a latitudinal segment through the Hudson Plains using circuitry analogues and our knowledge of peatlands in the Taiga Plains to characterize peatland complexes and how their form and hydrological function are changing due to permafrost thaw. This will be accomplished through the following specific objectives: (1) identify permafrost peatland forms, their position within peatland complexes, and contemporary distribution; (2) compare present-day and historical imagery over four decades, analyse land cover changes, and determine a latitudinal distribution of peatland complexes; (3) perform a systematic landform survey to characterize present-day peatland types, forms, and complexes over our entire latitudinal transect; (4) using the results of objectives 1–3, interpret the hydrological function of peatland complexes using circuitry analogues to generate an initial map of peatland complexes and landscapes vulnerable to change due to thaw.

2 | CONCEPTUAL APPROACH

Several authors have characterized the hydrological functioning of peatlands based on their physical form (e.g., Galkina, 1964; Galkina & Kiryushkin, 1969; Ivanov, 1975; Sjörs, 1959). Ivanov (1975) extended this causal relation between form and hydrological function to multiple spatial scales including what he referred to as the relatively low-order 'microforms' within individual peatlands (e.g., hummocks and hollows), the middle-order 'mires' (i.e., individual peatlands), and high-order 'mire massifs' (i.e., peatland complexes). Accordingly, the hydrological functioning of an individual peatland is affected by the form and therefore function of its component microforms, and the hydrological functioning of a peatland complex ($>10^0$ km^2 to $<10^1$ km^2) by the form and function of its component peatlands. Likewise, the hydrological functioning of a peatland-dominated landscape ($<10^2$ km^2) by that of its component complexes, and the hydrological functioning of a region ($>10^3$ 3 km^2) by the landscapes it contains.

By assigning specific hydrological functions of individual peatland types based on their form, we can infer hydrological flux and storage processes within and between peatlands and at the scales of peatland complexes and of landscapes containing multiple peatland complexes (i.e., 'compound mire massifs'; Ivanov, 1975). It has long been recognized that peatland complexes are deterministic features (Cajander, 1913; Ivanov, 1975; Sjörs, 1959; Vitt et al., 1994; Zoltai & Tarnocai, 1974) to the extent that their forms are shaped by the environmental conditions in which they developed (Waddington et al., 2015; Zoltai & Vitt, 1995). Therefore, as such conditions change, their forms also change (e.g., Kuhry, 2008), and presumably so too would their hydrological function. However, beyond consideration of how hydrological processes may change at specific locations is the need to understand how permafrost thaw affects the routing of water through a landscape of contrasting peatland forms and hydrological functions. Such scaling problems remain central questions in hydrology more broadly (Blöschl et al., 2019).

At smaller scales, there has been a substantial number of process-based studies that show the complexity of water movement in peatland soils (e.g., Beckwith et al., 2003; Quinton et al., 2009; Rezanezhad et al., 2016), microtopographic features (e.g., Balliston et al., 2018; McCarter & Price, 2017; Waddington et al., 2010), induvial forms (e.g., Branfireun & Roulet, 1998; Kværner & Kløve, 2008; Rouse, 1998), and complexes (e.g., Balliston & Price, 2022; Connon et al., 2015; Price & Maloney, 1994). Given feasibility limitations, process studies rarely examine the very large 'landscape' scale (e.g., Richardson et al., 2012), considered herein.

Hydrological functions are often conceptualized using electrical circuitry analogues (e.g., Dingman, 2002; Freeze & Cherry, 1979; Kirkham, 2005), because the flow of water and electricity are both governed by linear transport equations. Water flux is analogous to amperage in electrical terminology, storage to capacitance, and hydrological systems to circuits. Circuitry analogues offer insights into how water is routed through peatland landscapes, and how such routing will change as the landscape transitions in response to permafrost thaw (Figure 2). The electrical analogue has little practical value in most applications since it is always preferable to characterize and predict water flow and storage directly from knowledge of hydrological processes and pathways. However, defining the broad circuitry over landscapes is a good first step to understanding hydrological functioning at larger scales and will also help identify knowledge gaps and
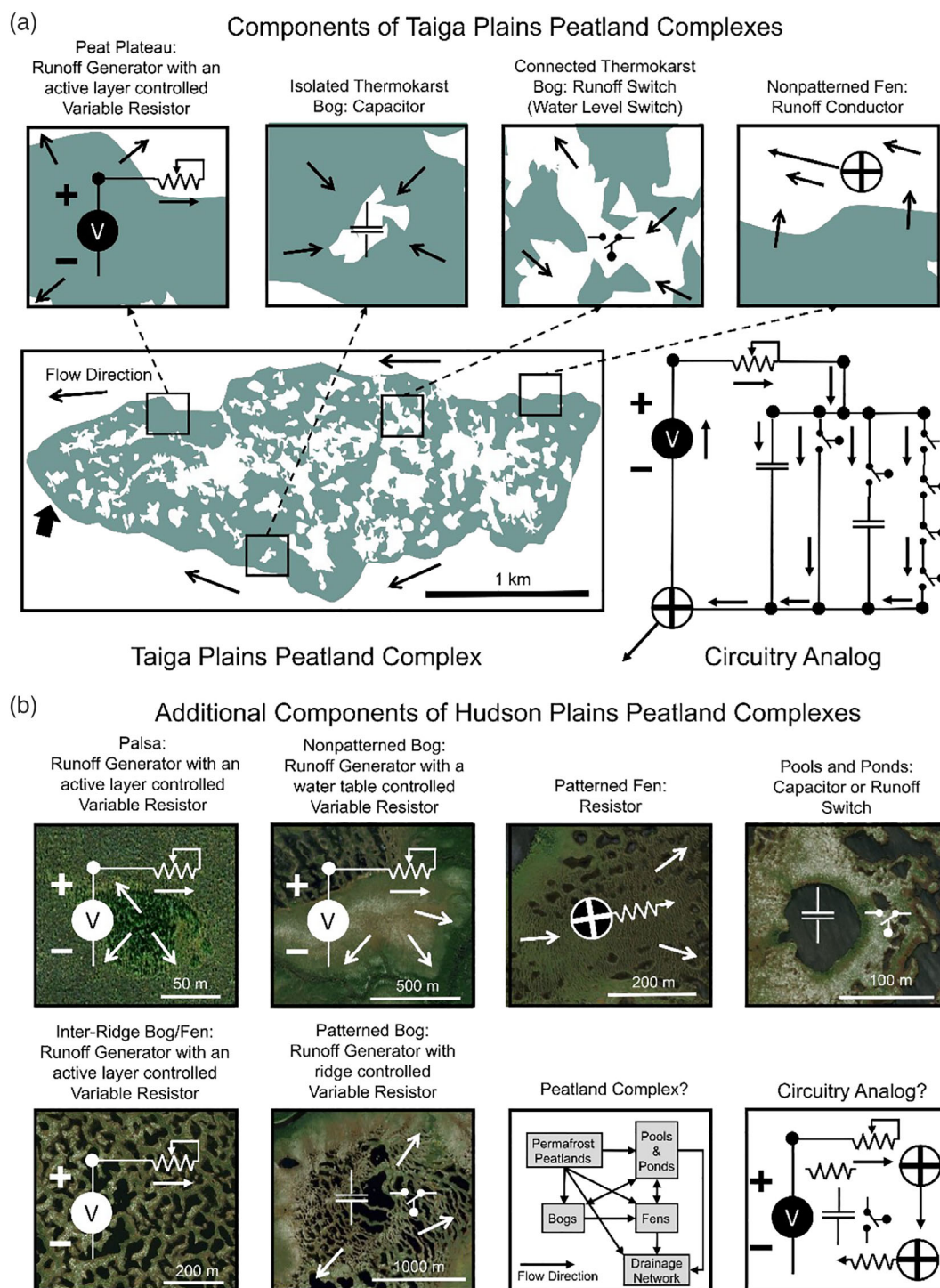
FIGURE 2 Components of peatland complexes in the Taiga Plains and Hudson Plains ecozones. For each landform, we show their hydrological function using a circuitry component symbol. For the Taiga Plains, all the components of the peatland complex (location: 61.36°N, 121.36°W) and circuitry analogue are known. For the Hudson Plains, there are additional peatland and circuitry components that occur. Hence, the peatland complexes and circuitry analogues are unknown. Note that for the Taiga Plains, both the peatland complex and circuitry analogue are present-day representations. Presumably, as the proportions of the peatland components change so too will the circuitry analogue.

needs. The electrical analogue also provides a framework to evaluate changes over time from historical aerial and satellite images. However, it must be stressed that while the analogue can ascribe general hydrological functions based on peatland form over large space and time scales, it is not intended to substitute information on specific processes and pathways arising from hydrological field studies. Rather it is used to identify general hydrological functions based on peatland form and position relative to other peatland forms. As such, it is

intended to complement detailed information on peatland hydrological functioning derived from field studies.

By occupying the highest topographic position in peatland complexes and owing to their impermeable frost table, permafrost peatlands function as run-off generators with an active layer (depth) controlled resistor (Quinton & Baltzer, 2013; Wright et al., 2008). While ephemeral connections between down-gradient collapse scar bogs, pools, and ponds are governed by water table thresholds, hence these forms function as water level switches (Kirpotin et al., 2009; Price & Maloney, 1994). In largely permafrost-free peatland complexes, bogs are often situated at the highest topographic position and are therefore run-off generators. However, the efficiency by which a bog generates run-off can be differentiated by whether it is patterned or nonpatterned. Patterned bogs have raised ridges and sunken hollows or pools arranged in repeating mosaics (Ivanov, 1975; NWWG, 1988; Riley, 2011) and therefore function as ridge-controlled run-off resistors. While nonpatterned bogs, which have microtopographic surfaces that are more similar to peat plateaus, function as water table (depth) controlled resistors.

The lower topographic position of fens relative to bogs ensures that run-off from peatland complexes flows through fens before entering the open-channel network (Price, 1987; Quinton et al., 2003). Like bogs, fens may be patterned or nonpatterned (Ivanov, 1975; NWWG, 1988; Riley, 2011). With more substantive microtopography, run-off from patterned fens encounters more barriers as it flows down-gradient, hence their hydrological function as run-off resistors (McCarter & Price, 2017; Quinton & Roulet, 1998). By contrast, with fewer barriers to down-gradient flow, nonpatterned fens function as run-off conductors (Quinton et al., 2003; Roulet & Woo, 1988). As a result, assuming similar flow path lengths (Beven & Kirkby, 1979), drainage densities (Dingman, 2002), and meteorological conditions, fen form governs the efficiency of water fluxes from permafrost peatlands to the open-channel network and onward to the basin outlet. Together, the occurrence and proportion of each peatland form (e.g., permafrost peatland, bog, fen) and their specific types (e.g., peat plateau, collapse scar bog, and patterned [net] fen) ultimately determines the hydrological function (i.e., wiring) of a peatland complex.

3 | STUDY REGION

Our primary Hudson Plains study region consists of a 300 km (8550 km²), from 52.8°N to 55.1°N latitudinal segment, which samples the sporadic, discontinuous, and continuous permafrost zones (Figure 1). The nearest, albeit sparsely distributed, climate stations with 1981–2010 data are Pickle Lake (51.45°N, 90.21°W) located 300 km to the south-southwest of our primary study area, Kuujjuarapik (55.28°N, 77.76°W) located 350 km east, Moosonee (51.29°N, 80.61°W) located 400 km east-southeast, and Gillam (56.36°N, 94.71°W) located 700 km west. From south to north within our study region, the mean annual air temperature ranges from 0.5 to −4.0°C, the mean annual precipitation ranges from 729 to 449 mm, the

percentage of precipitation falling as snow ranges from 28% to 36% (Environment and Climate Change Canada [ECCC], 2022), median peat thickness decreases from 2.2 to 0.6 m (Packalen et al., 2014), and post-glacial isostatic rebound increases from approximately 6 to 10 mm/year. (Henton et al., 2006).

4 | METHODS

4.1 | Imagery acquisition and classification: lidar transect

Parallel to and 45 to 100 km to the east of the primary study area is a 200-km lidar transect (Figure 1). The transect was part of a larger survey of Canada's boreal forest collected between June 14 and August 20, 2010, detailed descriptions, research motivations, data collection, and data processing are provided by Hopkinson et al. (2011), Milne et al. (2012), and Wulder et al. (2012). Metadata regarding the segment we interpreted is found in Table S2. Our analysis in ESRI (2018–2021) ArcMap 10.5–10.7 (Redlands, CA, USA) aimed to classify potential permafrost peatlands using the 1-m digital elevation model (DEM) that partially followed processes used by Chasmer et al. (2014). Major steps are presented in Figure 3a. Briefly, we aimed to delineate elevated surfaces (≥ 1 m above surroundings), which are indicative of permafrost peatlands in an otherwise low-relief terrain. We refined our initial classified image by manually removing elevated surfaces underlain by mineral substrates based on the Quaternary geology of Ontario shapefile (Pala et al., 1991). We then summarized our final classified image by 0.2°N latitudinal increments to facilitate our interpretation of the effects of latitude. We also used the classified lidar segment to cross-reference the visual appearance of permafrost peatlands on the other spectral imagery used in this study. Accuracy was evaluated by counting intersections between our classified image and 'ground truths'. These consisted of 100 elevation profiles distributed along the entire transect where an elevated surface occurred concurrently with a landform that upon visual inspection was indicative of a permafrost peatland.

4.2 | Imagery acquisition and classification: six areas of interest (AOIs)

We selected six AOIs, evenly spaced along a 300-km north-to-south transect from Kinusheo River in continuous permafrost to Koper Creek in sporadic permafrost to focus our analyses (Figure 1). Sutton Lake, North Washagami River, Ekwan River, and Muketei River comprised the intervening AOIs. Each AOI was 36 km², a feasible area for applying a manual classification in similar landscapes (e.g., Carpino et al., 2018) and consisted of recent high-resolution satellite imagery and historical air photos. The imagery was already atmospherically corrected and orthorectified, previously acquired by the Ontario Ministry of Natural Resources and Forestry or purchased from Digital-Globe (Westminster, Colorado, USA). Photos were purchased from
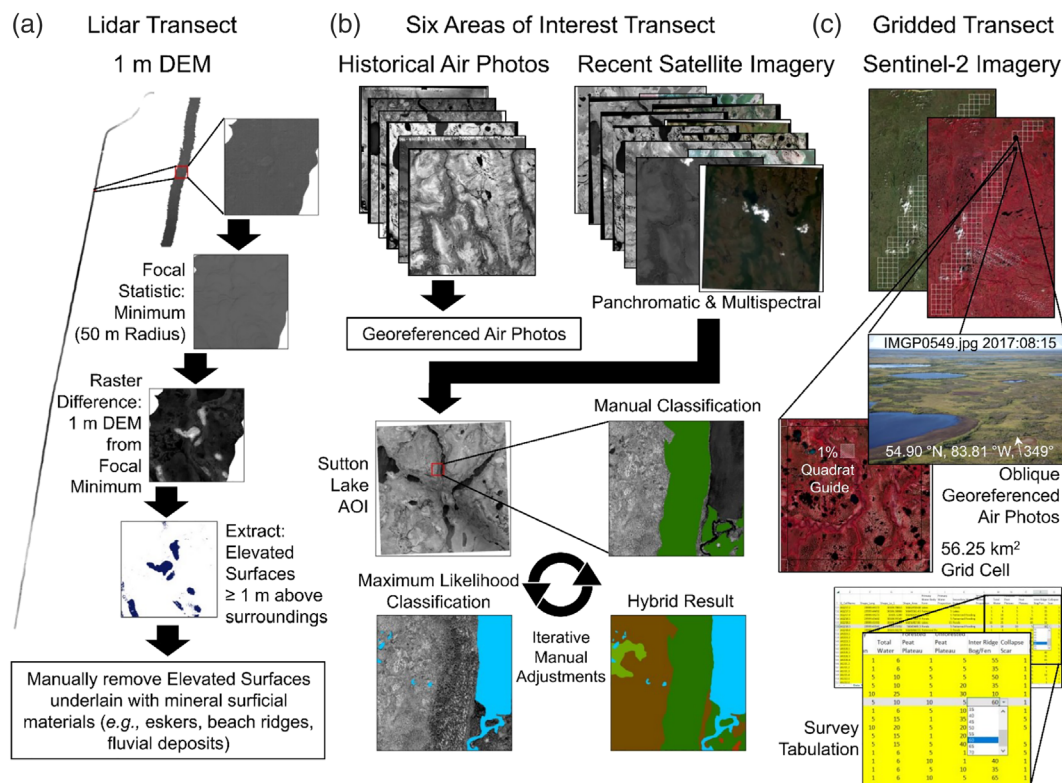
FIGURE 3 Simplified workflows depicting the major processing steps for analysing the (a) lidar, (b) six areas of interest, and (c) gridded transect.

the National Air Photo Library (NAPL, 2018) of Natural Resources Canada. Each AOI included distinct watercourses and/or waterbodies to aid with georeferencing photos in landscapes without static man-made structures (see Chasmer et al., 2010). The metadata for each satellite image and air photo is found in Table 1.

Initially, we manually classify land cover forms in each air photo and satellite image (Figure 3b). Where manual classification was deemed impractical (e.g., numerous waterbodies) or unsatisfactory (producer defined), we proceeded with algorithm-based classifications. First, we applied an iso-cluster unsupervised classification using 10–20 initial classes. If results were still unsatisfactory, a maximum likelihood supervised classification using between 10 and 50 training areas was implemented. For Kinusheo River, we used a segment mean shift object-based classification with spectral detail and spatial detail parameters both set to 20. We then manually edited all manual and algorithm-based classifications until we attained a satisfactory result for each photo and image. A complete accuracy assessment for each AOI classification is found in the Supporting Information document and includes an estimate of overall accuracy, the Kappa coefficient, confusion matrix, ground truths, commission, omission, user's, and producer's accuracies. To assess land cover changes, rather than directly subtracting our two classified images (i.e., exact spatial difference), we quantified proportional changes to each land cover form, and therefore did not calculate statistical significance. This approach was chosen because the incongruent alignment of air photos and satellite imagery where no static man-made structures exist results in

greater georeferencing error (Chasmer et al., 2010). Potential land cover forms for each AOI were water, forest, nonpatterned fen, patterned fen, nonpatterned bog, patterned bog, open permafrost peatland, beach/barren, and cloud. Forms were selected based on nomenclature found in Hudson Plains literature (NWWG, 1988; Ontario Ministry of Natural Resources and Forestry [OMNRF], 2014; Riley, 2011), potential usage as components of peatland complexes, and hydrological meaningfulness.

4.3 | Imagery acquisition and survey: gridded transect

To better understand the land cover patterns we observed among our AOIs, we also estimated land cover types across an overlapping transect using 10-m resolution Sentinel-2A imagery (Table S3) acquired using Google Earth Engine (Gorelick et al., 2017) (Figure 3c). Separately, in consultation with the Thermokarst Mapping Collective (see Gibson et al., 2021), we extended their 7.5 km × 7.5 km mapping grids covering the Northwest Territories (NWT), Canada to the Hudson Plains. The collective aims to create a systematic and broad-scale database describing the variation of thermokarst and periglacial features across the NWT using a grid-based framework and Sentinel-2A imagery. We concluded that applying a similar grid-based approach was favourable to performing a large-scale algorithm-based classification because our study was specifically interested in understanding

TABLE 1 Description of each 36-km^2 Hudson Plains area of interest (AOI) along the 300-km interrupted transect. Names are based on the nearest known waterbody or watercourse.

AOI name	KPR	MUK	EKW	NWG	SLK	KNS
Full name	Koper Creek	Muketei River	Ekwan River	North Washagami River	Sutton Lake	Kinusheo River
Latitude (centroid)	52.81°N	53.25°N	53.44°N	54.10°N	54.47°N	54.98°N
Longitude (centroid)	86.16°W	85.91°W	85.43°W	84.91°W	84.56°W	83.48°W
Distance from KPR (km)	NA	49	85	163	208	298
Distance between AOIs (km)	NA	49	36	78	45	90
Historical air photo name	24036_090	24469_063	24469_186	24471_131	24482_058	24472_167
Scale	1:60000	1:60000	1:60000	1:60000	1:60000	1:60000
Dots per inch (dpi)	1200	1200	1200	1200	1200	1200
Estimated resolution (m)	1.3	1	1.2	1.2	1.2	1
Georeferencing tie points	50	30	50	50	50	33
Georeferencing RMSE 1st-order polynomial (m)	5.5	2	4.8	4.0	4.5	2.6
Acquisition date	20 June 1975	22 June 1976	22 June 1976	29 June 1976	30 June 1976	1 July 1976
Recent imagery platform	WorldView-2	Deimos-2	GeoEye-1	Worldview-2	Worldview-3	Deimos-2
Panchromatic resolution (m)	0.5	1.0	0.5	0.5	0.3	1.0
Multispectral resolution (m)	2	1.0	1.8	2	1.2	1.0
Multispectral bands	8	4	4	8	8	4
Acquisition date	July 18, 2014	July 21, 2017	June 17, 2016	August 17, 2014	June 17, 2017	August 28, 2017
Time step (years)	39	41	40	38	41	41

the Hudson Plains landscape at a higher-order (i.e., peatland complexes) and structural perspective (i.e., patterned or nonpatterned) for which such classification techniques are not well suited.

Our gridded transect consisted of 152 grid cells centred on and inclusive of our six 36-km^2 AOIs (Figure 1). For each grid cell, we systematically moved around a 1% quadrat (750 m^2) as a reference, then using the Sentinel-2A imagery we estimated the proportion of each land cover type (Figure 3c). Land cover types were determined using available literature (Sjörs, 1959; Ivanov, 1975; NWWG, 1988; Radforth, 1969; Riley, 2011; Zoltai & Tarnocai, 1974; Zoltai & Vitt, 1995) and, where available, georeferenced oblique air photos ($N = 522$). Furthermore, our classified lidar image was used to cross-reference the visual appearance of permafrost peatlands relative to uplands on Sentinel-2A imagery. The minimum proportion assigned to any land cover type was 1%. Land cover types with greater proportions were estimated to the nearest 5% increment (i.e., 5% and 10%). Descriptions of each peatland form and type are provided in Table S1. Survey accuracy was assessed by performing two correlations between surveyed and classified land cover results within our 36-km^2 AOIs. The first, compared land cover forms among AOIs (i.e., water and forest). The second, compared survey and classified land cover forms within AOIs (i.e., Kinusheo River [classified] vs. Kinusheo River [surveyed]). We used Pearson's correlation coefficients unless a Shapiro–Wilk's test of normality ($\alpha = 0.01$) suggested that a Spearman's rank correlation was more appropriate (R Core Team, 2022).

4.4 | Mapping peatland complex and landscape vulnerability

We defined vulnerability based on Chapin et al. (2004), as systems more sensitive to change following subjection to a disturbance. Therefore, in each grid cell, we evaluated the vulnerability of the most prevalent peatland complex to increased hydrological response (i.e., more sensitive to change) as permafrost thaws (i.e., a disturbance) over the coming decades. The vulnerability was ranked into four categories, most, more, less, and least using a decision tree (Figure 4). Grid cells were ranked as most vulnerable where peatland complexes were composed of ≥35% permafrost peatland areal and where nonpatterned fens were the most prevalent fen form (i.e., Taiga Plains like). Grid cells were given the rank of least vulnerable where permafrost peatlands account for <35% areal. We chose 35% as a conservative first approximation for minimum permafrost peatland area for landscapes to be vulnerable to hydrological change in the Hudson Plains because the percentage reflected estimates from the southern sporadic permafrost zone of the Taiga Plains where such changes occurred (Carpino et al., 2021). We assigned intermediary vulnerability ranks based on whether the most prevalent fen forms in each grid cell were patterned (terraced) fens or patterned (net) fens, which corresponded to the ranks of more and less vulnerable, respectively. Assigning a higher vulnerability to patterned (terraced) fens acknowledges their steeper slopes and more efficient flow paths relative to patterned (net) fens (Table S1).
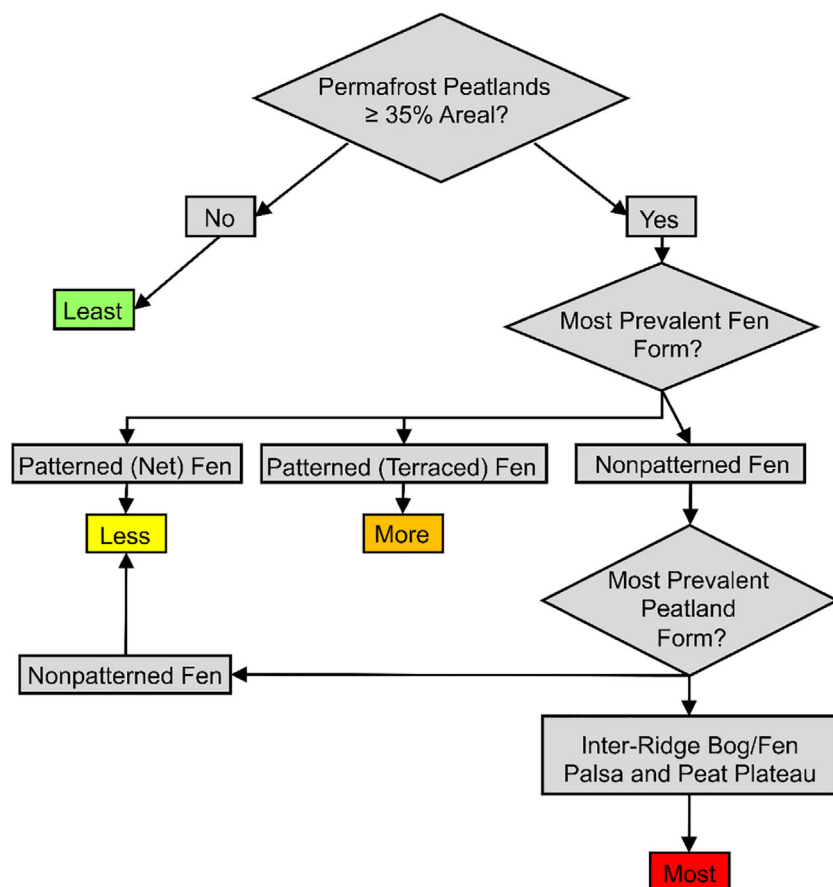
FIGURE 4 Decision tree used for mapping peatland complex and landscape vulnerability to permafrost-thaw-induced hydrological change.

5 | RESULTS

5.1 | Latitudinal trends of permafrost peatland area estimates

Our lidar classification demonstrated that permafrost peatlands were present throughout the sporadic (Figure 5a) and discontinuous permafrost zones (Figure 5b) but occupied only a minor area within the overall landscape. We observed that permafrost peatlands were positioned either as 'islands' within larger permafrost-free peatland complexes or on the periphery of watercourses and waterbodies. For every 0.2°N latitudinal increment in the sporadic (52.5°N to 53.7°N), we estimated permafrost peatland area accounted for between 3% and 18% (mean = 8.1%) of total land cover with no clear latitudinal trend (Figure 5c). For every 0.2° latitudinal increment in the southern discontinuous (53.7°N to 54.2°N) we estimated permafrost peatlands accounted for between 2% and 12% (mean = 8.3%) of total land cover (Figure 5c). Approximately 89% of the 'ground-truth' elevation profile graphs for the sporadic and discontinuous zones coincided with a 'permafrost peatland' derived from lidar classification. Sources of commission were the misclassification of shorelines (N = 8) and uplands (N = 3).

5.2 | Latitudinal and temporal variation of peatland forms

Classifications of recent (2014, 2016, and 2017) imagery demonstrated several distinct latitudinal patterns at the peatland form hierarchical level. Bogs were the most prevalent peatland forms in four out of six AOIs (Table 2, Figure 6), including Koper Creek, Ekwan River, North Washagami River, and Sutton Lake. While fens were the most prevalent peatland forms in, the Muketei River and the Kinusheo River AOIs. Nonpatterned bogs accounted for at least 90% of all bog forms, whereas nonpatterned fens accounted for less than 20% of all fen forms. Waterbodies occupied substantial areas in Ekwan River, Sutton Lake, and Kinusheo River. Forest cover, which includes treed permafrost peatland forms, was greatest in Kinusheo River and Sutton Lake, followed by North Washagami River, Koper Creek, Muketei River, and Ekwan River. Permafrost is known to be continuous in Kinusheo River, our estimated open permafrost peatland and forest areas were 7% and 32%, respectively, suggesting that most of the permafrost occurs in mineral substrates below nonpatterned fens (41% areal) and waterbodies (19% areal). Based on visual inspection, we highly suspect there were open permafrost peatland forms in Sutton Lake and North Washagami River, but without an ability to confirm
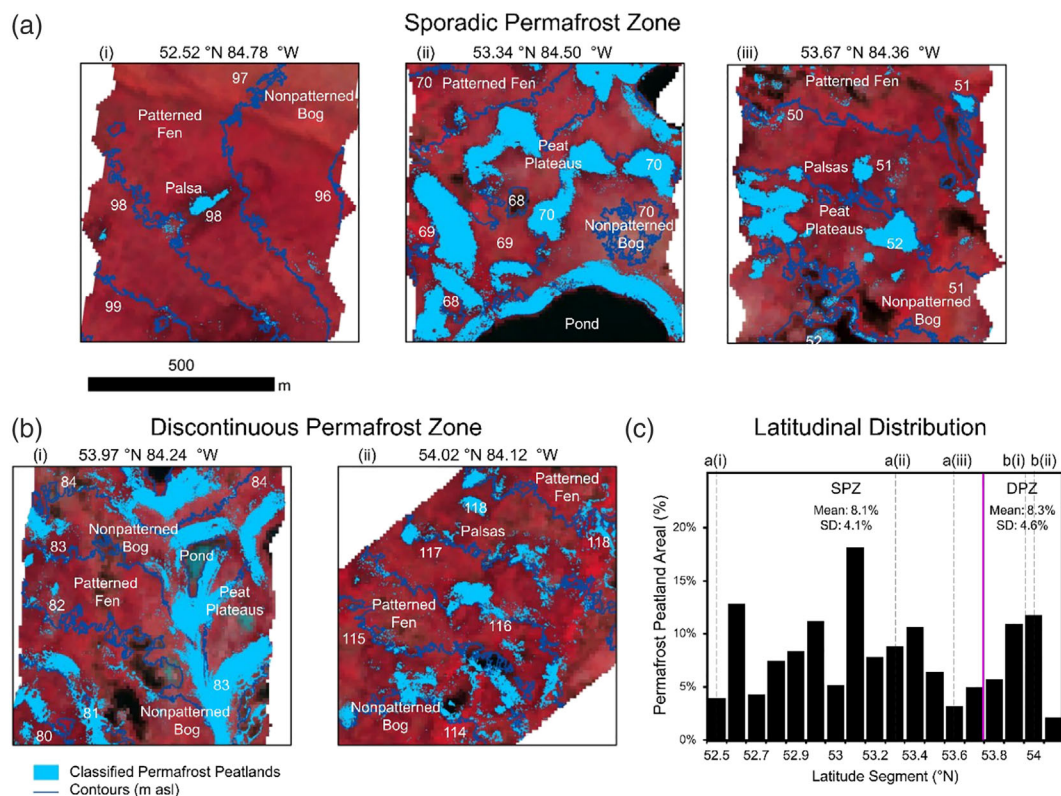
FIGURE 5 Images (750 m × 750 m) are examples of lidar-classified permafrost peatlands along a 200 km (~135 km2) latitudinal transect in the (a) sporadic (SPZ) and (b) discontinuous permafrost (DPZ) zones of the Hudson Plains. (c) The bar graph depicts the estimated area of permafrost peatlands for each 0.2°N of latitude, the latitude segment where examples are found, and descriptive statistics for the transect segments in the sporadic and discontinuous permafrost zones.

TABLE 2 Summary of land cover forms classified in each Hudson Plains area of interest (AOI) using recent satellite imagery arranged from south to north.

Land cover	Water	Forest	Nonpatterned fen	Patterned fen	Nonpatterned bog	Patterned bog	Open permafrost peatland	Burn	Beach/ barren	Cloud
AOI	(%)	(%)	(%)	(%)	(%)	(%)	(%)	(%)	(%)	(%)
Koper Creek	0	11	1	18	62	6	0	0	0	2
Muketei River	0	8	8	41	40	2	0	0	0	0
Ekwan River	18	2	0	22	56	1	0	0	0	0
N. Washagami River	5	13	0	23	28	1	0	29	0	1
Sutton Lake	10	25	2	12	45	1	0	5	0	0
Kinusheo River	19	32	41	0	0	0	7	0	< 1	0

using ground verification or lidar classification, those landforms were classified as a nonpatterned bog.

Since the mid-1970s, forest cover (a proxy for permafrost peatlands) decreased and nonpatterned bogs increased by less than 5% of the total areas, in the sporadic zone and southern part of the discontinuous zones (Figure 6). However, in Koper Creek, our most southern AOI, several treed permafrost peatlands present in 1975 were completely degraded by 2014 (Figure S1f). In contrast, forest cover

decreased by 9% to 16% in the northern discontinuous permafrost zone. In Kinusheo River, our comparison showed losses to water (−1%) and nonpatterned fen (−3%) areas, gains to the forest (+3%) and to open permafrost peatland (+1%) areas (Figure 6), despite the observed breakup of several large open permafrost peatlands (Figure S1a). We suspected that the low spectral contrast observed between open permafrost peatland and nonpatterned fen forms in the 1976 air photo was the cause. When we recalculated open
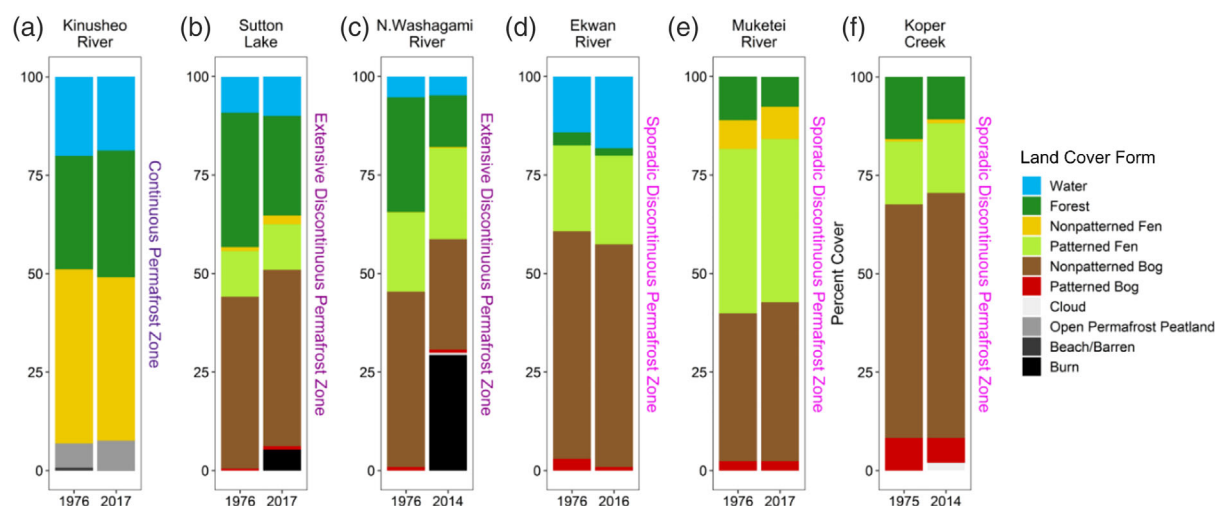
FIGURE 6 Stacked bar plots showing the percentage of land cover forms between a classified air photo and satellite image. Hudson Plains areas of interest (AOIs) are arranged from northernmost (furthest left) to southernmost (furthest right).

AOI Year	Koper Creek		Muketei River		Ekwan River	
	1975	2014	1976	2017	1976	2016
Classification method	MC	MC	MC	MC	HYB	HYB
Overall accuracy	86.1%	91.4%	95.5%	94.5%	93.3%	93.5%
Kappa coefficient	79.3%	89.8%	94.3%	93.1%	91.3%	91.4%
AOI Year	N. Washagami River		Sutton lake		Kinusheo River	
	1976	2014	1976	2017	1976	2017
Classification method	HYB	HYB	HYB	HYB	SMS	SMS
Overall accuracy	95.0%	92.3%	90.9%	90.4%	86.5%	89.4%
Kappa coefficient	93.7%	90.3%	88.9%	88.3%	82.6%	86.3%

TABLE 3 Summary of land cover classification accuracy assessments and the classification method used for the six areas of interest in the Hudson Plains. For each image, the final classification reflected the best overall result of a manual classification (MC), a hybrid (HYB) approach using a manual classification and iso cluster unsupervised classification or a maximum likelihood supervised classification, or a segment mean shift (SMS) object-based classification.

permafrost peatland losses only within their classified bounds from the 1976 classified air photo, we then found a loss of 2% by 2017 (Figure S2).
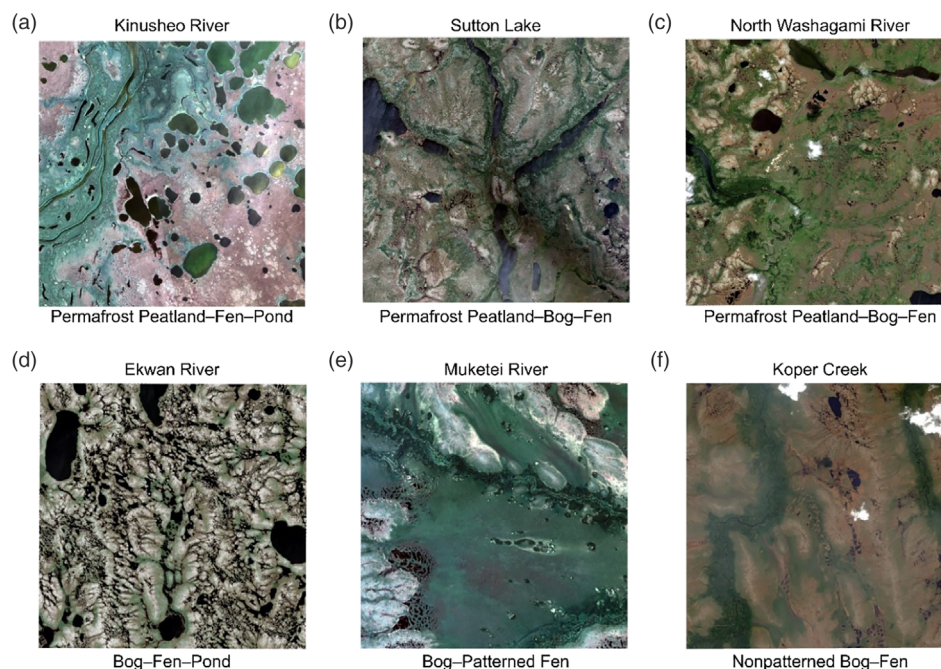
In addition to permafrost-thaw-induced disturbances, we also observed the impacts of wildfires in Sutton Lake and North Washagami River. Using Landsat 5 TM imagery to highlight recently burned vegetation and the most up-to-date National Fire Database (NFDB, 2022) we estimated the total area burned and dates for each wildfire (Figure S3) and amended Table 2 and Figure 6 to include burned area (black). In Sutton Lake, a 1.9-km^2 wildfire occurred in June 1995 (NFDB, 2022). The wildfire burned 0.7 km^2 of forest, 1.1 km^2 of nonpatterned bog, and 0.1 km^2 of patterned fen areas. In North Washagami River, a 10.5-km^2 wildfire occurred between July–September 2003 (NFDB, 2022). The wildfire burned 4.2 km^2 of forest, 6.0 km^2 of nonpatterned bog and 0.3 km^2 of patterned fen areas. Based on our burned area analyses, the remaining 78% (2.5 km^2, 7% areal) and 60% (6.4 km^2, 10% areal) of all forest losses in Sutton Lake and North Washagami River, respectively, resulted from permafrost-thaw-induced disturbances. For each classified AOI image ($N = 12$),

the overall accuracies and Kappa coefficients were between 79% and 86% (Table 3).

5.3 | Identification of peatland complex types

Using the most prevalent run-off generating and run-off conducting (see Figure 2) peatland forms (see Table S1) classified in each AOI, we identified the following peatland complexes (Figure 7a–f): For Kinusheo River (a), permafrost peatland–fen–pond; for Sutton Lake (b) and North Washagami River (c), permafrost peatland–bog–fen; for Ekwan River (d), bog–fen–pond; for Muketei River (e), bog–patterned fen; for Koper Creek (f), nonpatterned bog–fen. Each identified peatland complex corresponds to the most prevalent, not the exclusive peatland complex found within each AOI, while the sequence of land cover forms in each identified peatland complex (e.g., bog, fen, and pond) corresponds to the overall topographic gradient among the two or three forms, and therefore, the surface or near-surface preferential flow paths.

FIGURE 7 A 'true colour' (red, green, blue) composite satellite image for each Hudson Plains area of interest (see Figure 1) using the multispectral bands from their respective satellite platform (see Table 1). Each (6 km × 6 km) AOI is labelled by the primary peatland complex. Note that Sutton Lake, North Washagami River, and Ekwan River images were each rotated 2°, 1.5°, and 1.5° counterclockwise, respectively, to align with the other AOIs.

(a) Kinusheo River — Permafrost Peatland–Fen–Pond

(b) Sutton Lake — Permafrost Peatland–Bog–Fen

(c) North Washagami River — Permafrost Peatland–Bog–Fen

(d) Ekwan River — Bog–Fen–Pond

(e) Muketei River — Bog–Patterned Fen

(f) Koper Creek — Nonpatterned Bog–Fen

5.4 | Latitudinal land cover trends and comparison to classified AOIs

Within our 8550-km^2 gridded transect open, nonpatterned fens (see Table S1), rapidly transitioned from more than 50% of the total area at 55.0°N to less than 5%at 54.7°N. (Figure 7). Open, nonpatterned fens were surrounded by open, inter-ridge bogs/fens and peat plateau fields. These peatland types, along with the numerous pools and ponds form widely dispersed often multisquare kilometre heterogeneous peatland complexes. Open, inter-ridge bogs/fens and peat plateau fields contributed nearly 50% to the total land cover area and were most common near the continuous–discontinuous transition zone (54.7°N), and steadily declined southward, stretching into the sporadic permafrost zone (53.8°N). Over the same latitudinal range, we observed large areas of forest and peatland, which showed signs of past wildfires, accounting for nearly 50% of the total land cover at 54.3°N. Treed peat plateaus contributed nearly 20% of the total land cover area at 54.3°N and were the only permafrost peatland type to occupy areas >1% south of 53.8°N. Thaw disturbances/collapse scars (Harris et al., 1988) occurred throughout the transect adjacent to many permafrost peatlands and occupied a maximum of 10% of the total land cover at 53.5°N. Overall, we found that open, nonpatterned bogs and treed, patterned (terraced) fens (see Table S1) were the most prevalent permafrost-free peatland types and, therefore, were important components of our identified peatland complexes. Open, nonpatterned bog area contributed nearly 45% to the total land cover area at 53.6°N, while further south, treed, patterned (terraced) fen area contributed nearly 20% to the total land cover area at 53.3°N. Comparing all surveyed and classified land cover forms (i.e., one hierarchal level above land cover type) and within each AOI, correlations were all greater than 0.76 (Table 4).

TABLE 4 Correlation summary between classified and surveyed Hudson Plains land cover forms and among areas of interest. Land cover types from survey results were combined into their land cover forms prior to calculating correlations. Correlations were statistically significant at p values <0.01 (*), <0.001 (**), and <0.0001 (***).

Correlation variable	Estimate	p-value	Correlation type
Water	0.98*	6.07×10^{-4}	Pearson's r
Forest/burn	0.95*	3.33×10^{-3}	Pearson's r
Nonpatterned bog	0.9	1.43×10^{-2}	Pearson's r
Patterned bog	0.77	7.50×10^{-2}	Pearson's r
Nonpatterned fen	0.77	7.23×10^{-2}	Spearman rank
Patterned fen	0.96*	2.45×10^{-3}	Pearson's r
Permafrost peatland	0.77	7.05×10^{-2}	Spearman rank
Kinusheo River	0.97**	3.77×10^{-4}	Pearson's r
Sutton Lake	0.95*	1.11×10^{-3}	Pearson's r
N. Washagami River	0.98**	1.37×10^{-4}	Pearson's r
Ekwan River	0.99***	6.87×10^{-6}	Pearson's r
Muketei River	0.76	4.89×10^{-2}	Spearman rank
Koper Creek	0.9*	5.62×10^{-3}	Spearman rank

6 | DISCUSSION

6.1 | Apparent hydrological function

The hydrological function of peatland complexes has previously been conceptualized by applying the fill-and-spill concept to permafrost (Connon et al., 2015) and permafrost-free (McCarter & Price, 2017) settings. Fill-and-spill described run-off controlled by a stepwise expansion of contributing areas as storage thresholds in individual

soil-filled valleys surrounded by Canadian Shield bedrock hydrologically connected (Spence & Woo, 2003, 2006). Because topographically abrupt and impermeable geological barriers (i.e., Precambrian bedrock) control storage thresholds in Canadian Shield landscapes and topographically subtle and permeable biophysical barriers (i.e., peatland microtopography) control those in peatland complexes, there are limitations to applying fill-and-spill. For example, McCarter and Price (2017) demonstrated a non-stepwise expansion of contributing areas in a patterned fen with ridge-flark microtopography, where ridge transmissivity increased exponentially as the water table rose into the upper 0.1 m of peat. Furthermore, Balliston and Price (2022) in a patterned bog-fen complex showed that warmer-than-average springtime temperatures accelerated snowmelt faster than seasonal frost could sufficiently thaw in the fen, allowing snowmelt run-off from the bog to short-circuit and flow into the stream channel without replenishing fen storage. Consequently, during the summertime, hydrological connectivity was lower and threshold requirements were higher.

In addition to the abovementioned fill-and-spill limitations, field-based hydrological processes studies are spatially limited, hence, we suggest applying circuitry analogues to understand the potential hydrological vulnerability of peatland complexes as permafrost thaws at the landscape and regional scale. Although circuitry analogues cannot be used to provide insights into specific hydrological processes or interannual hydrological variability within peatland complexes and their component forms, they do demonstrate latitudinal patterns in landscape structure (i.e., circuitry wiring) and how such structure may respond to a disturbance (i.e., permafrost thaw).

The high correlations between our classified and surveyed results (Table 4) suggest that the five peatland complexes identified in each classified AOI (Figure 7) are representative of the larger landscape and therefore their form and function relationships are scalable. For each complex-specific circuitry analogue (Figure 9),

amperage, analogous to run-off, is described as dispersed in complexes with many small individual run-off generators, concentrated in complexes with a few large run-off generators, and reduced in complexes with highly resistive run-off generators and/or circuitry. Each circuitry analogue is adaptable to complex specific variations in their component forms. Furthermore, each circuitry analogue is nonstationary as disturbances can shift peatland components from one form to another, altering component proportions and in doing so, changing circuitry and total amperage. Disturbances may be shorter term like permafrost thaw and wildfire or longer term like peatland succession and isostatic rebound.

6.2 | Vulnerability map

Using the decision tree outlined in Figure 4, our initial map of landscape vulnerability to permafrost-thaw-induced hydrological change in the Hudson Plains is shown in Figure 10a and suggests a 60-km latitudinal segment (54.5°N to 54.9°N) where peatland complexes are most vulnerable. We assert that each 56.25-km² grid cell represents the landscape scale because they contain multiple peatland complexes (Figure 1). Landscapes where complexes are characterized as permafrost peatland–fen–pond or permafrost peatland–bog–fen corresponds to the most, more, and less vulnerable (Figure 10b). All other landscapes are ranked as least vulnerable and occur mainly in the sporadic permafrost zone and parallel the lidar transect (Figure 5). Because fen form controls run-off efficiency (Quinton et al., 2003; Quinton & Roulet, 1998), among the permafrost peatland complexes the most prominent fen form further discriminates between landscapes most vulnerable (non-patterned), more vulnerable (patterned and terraced), and less vulnerable (patterned and net) (see Table S1). An exception is found in the continuous permafrost zone where non-patterned fens are the most prevalent of all peatland forms (Figure 8;
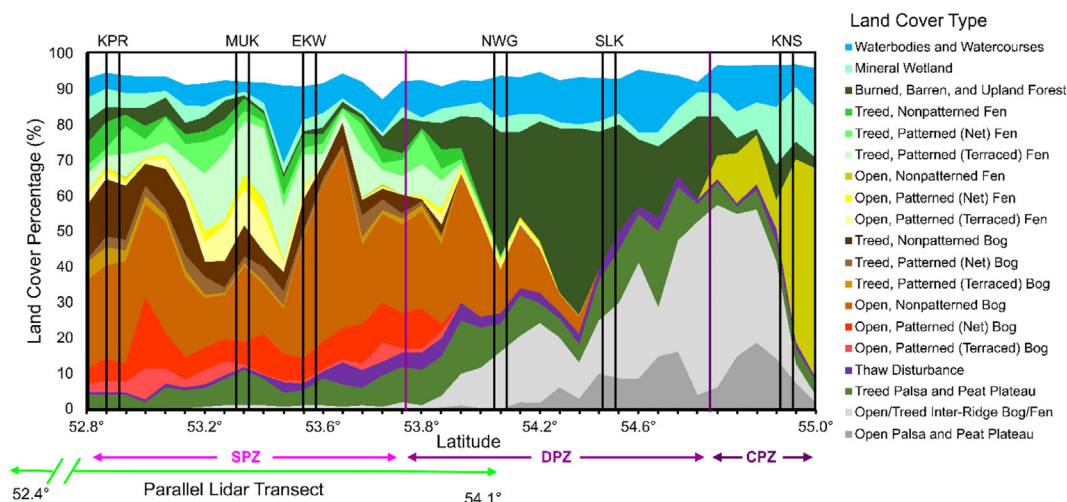

FIGURE 8 Area plot of Hudson Plains land cover types. Land cover is summarized by grid row (four grid cells per row). The locations of the six AOIs are shown with solid black line boxes and the approximate boundaries between permafrost zones are shown with dashed lines. An estimated 5%–10% uncertainty exists across all grid cells (white area).

Figure 10b). In such landscapes, we substantially reduced vulnerability from most to less (Figure 10a), because the development of new flow paths as permafrost peatlands thaw would be spatially limited (e.g., Figure 7a; Figure S2).

6.3 | Latitudinal land cover trends and temporal variation

Concerning the distribution of permafrost peatlands in the Hudson Plains and quantifying the rate and pattern at which these landforms are thawing, previous studies and this study suggest that in the ecoregion's sporadic permafrost zone, permafrost peatlands occupy <5%–15% areal (Figure 5), consist primarily of treed permafrost peatlands (Figure S1), and have thawed between 0.08%–0.79% decade^{-1} (Figure 6). One study by Pironkova (2017) compared air photos to satellite imagery between the mid-1950s and 2011 (56/57 years) and found that permafrost peatlands decreased from 4.5% areal to 3.3% areal (−1.2%) in a 435-km^2 landscape. Over a 7861-km^2 landscape, a model by Ou et al. (2016) estimated 9.4% permafrost areal using moderate resolution imagery (30 m) in combination with soil temperature

and climate data. Their study also hindcast to estimate permafrost area between 1960 and 1969 at 9.8%, a margin difference of 0.4% over five decades that was attributed to the resilience of thick and well-insulating peat soils. Those permafrost losses are less than our estimates of total forest loss (a proxy for permafrost peatlands) in Koper Creek (−3.9%) between 1975 and 2014 (40 years), and Muketei River (−3.3%) between 1976 and 2016 (42 years) (Figure 6), which fall within the sporadic permafrost zone.

We posit that the range of permafrost area estimates reflects the uneven distribution of permafrost peatlands across the sporadic permafrost zone as seen in our lidar analysis (Figure 5). However, given that the longitudinal width of our lidar surface ranged from 600 to 900 m, sampling error was certainly a contributing factor to our estimates. The larger losses in forest cover in this study may reflect a sampling error as well because we selected AOIs near distinct water bodies for georeferencing purposes where thaw rates were highest in the Pironkova (2017) study or accelerating permafrost thaw over the warmest decade (2010–2019) on record (National Oceanic and Atmospheric Administration [NOAA], 2022), or both. Nevertheless, such marginal losses (Figure 6d–f) and limited permafrost extent (Figure 8) in the southern portion of our study area support ranking these
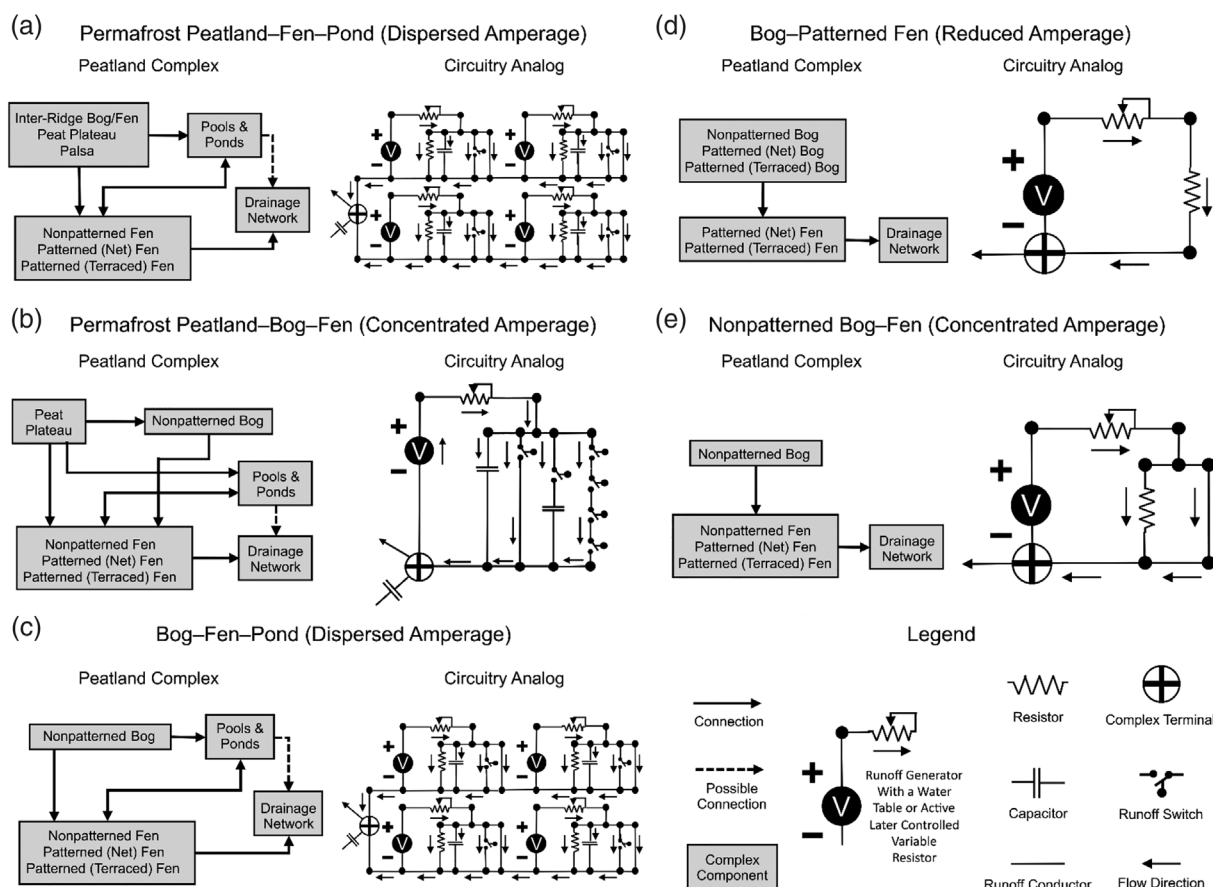

FIGURE 9 Peatland complexes identified in the Hudson Plains study region, their components, and circuitry analogues. Circuitry analogues indicate all potential flow paths through a peatland complex.

landscapes as least vulnerable (Figure 10a) because their landscape structure and therefore circuitry will not change substantially as permafrost thaws (Figure 9c–e).

Further north, we observed losses to permafrost peatlands in both the discontinuous (7%–10%) (Figure 6) and continuous (2%) permafrost zones (Figure S2). Losses are greater than those by Zhang et al. (2012) who modelled active layer thickness (ALT) and permafrost area in a peatland complex landscape approximately 670 km northwest of our study area. They estimated that over 100 years (from 1900–1909 to 2000–2009) permafrost thaw was 2.8% areal and exclusively occurred in the discontinuous permafrost zone. The marginal losses reflected the more northerly location of their study and the high threshold, modelled ALT greater than 4 m, used to determine permafrost thaw. The greater losses we observed, particularly in the discontinuous permafrost zone, reflect areal changes to permafrost landforms as opposed to ALT and the more southern location of our study area. Such observed (Figure 6) and potential (Figure 8) changes to landscape structure and therefore circuitry (Figure 9a,b) support the ranking of these landscapes as either more or most vulnerable (Figure 10a), depending on which fen forms are most prevalent (Figure 10b).

Outside of the Hudson Plains, studies have largely found greater rates at which permafrost peatlands have recently thawed.

For example, in the sporadic and discontinuous zones of Québec's Taiga Shield and Southern Arctic ecozones, Payette et al. (2004) found that 80% of the permafrost in an inter-ridge bog/fen had thawed over 47 years (1957–2004), and further north, Vallée and Payette (2007) found that 23% of palsa areas had thawed over 44 years (1957–2001). Similar latitudinal patterns and even greater permafrost thaw rates have been described in Lapland (Luoto & Seppälä, 2002, 2003). In the Taiga Plains, Carpino et al. (2018) found that forest area losses between 1970 and 2010 along a 200-km latitudinal transect in the sporadic permafrost zone ranged from 6.9% to 11.6%, with greater losses observed further north. Despite measuring smaller areal changes to permafrost peatlands in the Hudson Plains compared to other permafrost regions, patterns of permafrost thaw in peatland landscapes appear similar. Generally, a greater proportion of thaw-related disturbances occur in the northern sporadic and southern discontinuous permafrost transition zone (Figure 6; Figure 8), where permafrost peatlands are more abundant compared to regions further south but are more strongly experiencing the effects of warming temperatures compared to landscapes further north. We reflected this general pattern in the vulnerability map insofar as discriminating between landscapes least and less vulnerable immediately north of sporadic-discontinuous transition (Figure 10a).
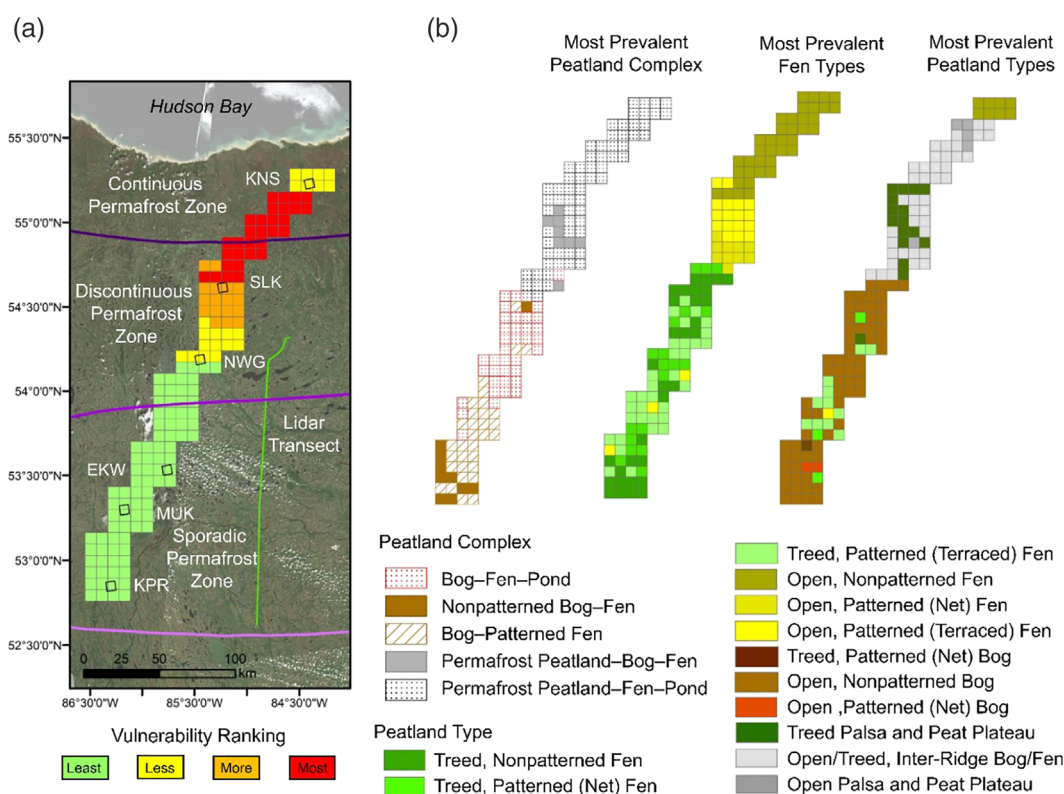

FIGURE 10 (a) Vulnerability map of peatland complexes in the Hudson Plains to permafrost thaw-induced hydrological change annotated with the locations of the lidar transect, six 36-km^2 AOIs, and permafrost zones. (b) Distribution of the most prevalent peatland complexes, fen types, and peatland types in each grid cell, which together with the decision tree (see Figure 4) were used to determine vulnerability in each grid cell.

6.4 | The Hudson Plains and Taiga Plains compared

Studies in Taiga Plains have shown that to increase hydrological response, peatland complexes must be initially composed of a substantial area of permafrost peatlands, permafrost thaw must form enough new hydrological pathways to increase the contributing area of the landscape, and fens must not inhibit new pathways from reaching the basin outlet. For example, Connon et al. (2014) showed that a 33% increase in contributing area (from 31.1% to 41.8%) and a 137 mm increase in run-off occurred over two decades in a landscape initially composed of 54.6% permafrost peatlands rapidly decreases to 47.5% (−7.1%) over 34 years (1977–2012). Areal permafrost losses in Sutton Lake (−10%) and North Washagami River (−7%) were like those measured by Connon et al. (2014); however, neither landscape was initially composed of >40% permafrost peatlands and each contained more patterned than nonpatterned fens (Figure 6). These structural differences highlight their reduced vulnerable rankings (Figure 10a). Despite only a small proportion of peatland complexes in our study area resembling those in Taiga Plains, that is, permafrost peatland–bog–fen (concentrated amperage) complexes, we assert that this does not preclude permafrost peatland–fen–pond (dispersed amperage) complexes from undergoing increased hydrological response as permafrost thaws, so long as they meet the conditions described above. However, for either peatland complex, what remains uncertain and what circuitry analogues cannot determine is which complexes will connect to the larger drainage network and which to isolated waterbodies as permafrost thaws (see Kirpotin et al., 2009).

7 | CONCLUSION

We characterized peatland complexes along a 300-km latitudinal segment in the Hudson Plains using multiple remote sensing approaches, conceptualized their hydrological function using circuitry analogues, and assessed their vulnerability to permafrost-thaw-induced hydrological change based on those conditions and estimated land cover changes. Out of the five peatland complexes we identified, two had sufficient permafrost peatland proportions (≥35%, areal) to suggest some vulnerability to permafrost-thaw-induced hydrological change, permafrost peatland–fen–pond (dispersed amperage) and permafrost–bog–fen (concentrated amperage). We suggested the most vulnerable landscapes occur where nonpatterned fens were the most prevalent fen form, not the most prevalent peatland form. Based on these parameters, we identified a 60-km latitudinal segment (54.5°N to 54.9°N) where landscapes are most vulnerable and should therefore be the focus of future research and monitoring efforts in the Hudson Plains of northern Ontario. Conceptualizing the hydrological function of peatland complexes using circuitry analogues indicated which complexes and landscapes in the Hudson Plains were most vulnerable to increased hydrological response as permafrost thaws.

However, because each circuitry analogue represents a nonspecific peatland complex, the analogues cannot be used to determine if individual peatland complexes were vulnerable or used as routing networks in hydrological models. This study has highlighted an ongoing challenge, which is the juxtaposition between the large scale (10^2 km^2) of the Hudson Plains which necessitates remote sensing approaches and the heterogeneity of peatland components over small scales (10^{-3} km^2) which impedes classification of individual permafrost peatlands without the use of high-resolution satellite imagery. Furthermore, because patterned peatlands are composed of several land cover types, algorithm-based classifications are ineffective at delineating their bounds. We know that as permafrost thaws, the hydrological function of individual permafrost peatlands changes. At some critical threshold, hydrological changes aggregate so that the hydrological response of entire peatland complexes, landscapes, and regions changes. Therefore, future work should aim to decipher peatland complexes that may connect to the drainage network as permafrost thaws, and which will not.

DATA AVAILABILITY STATEMENT
The data that support the findings of this study are available from the corresponding author upon reasonable request.

ORCID
Mikhail Mack https://orcid.org/0000-0001-7257-9398

REFERENCES

Balliston, N., & Price, J. S. (2022). Beyond fill and spill: Hydrological connectivity in a sub-arctic bog-fen-tributary complex in the Hudson Bay Lowlands, Canada. *Hydrological Processes*, *36*(4), e14575. https://doi.org/10.1002/hyp.14575

Balliston, N. E., Patrick, C., McCarter, R., & Price, J. S. (2018). Microtopographical and hydrophysical controls on subsurface flow and solute transport: A continuous solute release experiment in a subarctic bog. *Hydrological Processes*, *32*, 2963–2975. https://doi.org/10.1002/hyp.13236

Beckwith, C. W., Baird, A. J., & Heathwaite, A. L. (2003). Anisotropy and depth-related heterogeneity of hydraulic conductivity in a bog peat. I: Laboratory measurements. *Hydrological Processes*, *17*(1), 89–101. https://doi.org/10.1002/hyp.1116

Beven, K. J., & Kirkby, M. J. (1979). A physically based, variable contributing area model of basin hydrology. *Hydrological Sciences Bulletin*, *24*(1), 43–69. https://doi.org/10.1080/02626667909491834

Blöschl, G., Bierkens, M. F. P., Chambel, A., Cudennec, C., Destouni, G., Fiori, A., Kirchner, J. W., Mcdonnell, J. J., Savenije, H. G., Sivapalan, M., Stumpp, C., Toth, E., Carr, G., Lupton, C., Salinas, J., Széles, B., Aksoy, H., Allen, S. T., Amin, A., ... Yilmaz, K. K. (2019). Twenty-three unsolved problems in hydrology (UPH)—A community perspective. *Hydrological Sciences Journal*, *64*(10), 1141–1158. https://doi.org/10.1080/02626667.2019.1620507

Branfireun, B. A., & Roulet, N. T. (1998). The baseflow and storm flow hydrology of a Precambrian shield headwater peatland. *Hydrological Processes*, *12*(1), 57–72. https://doi.org/10.1002/(SICI)1099-1085(199801)12:1<57::AID-HYP560>3.0.CO;2-U

Brown, J. O., Ferrians, J. A., Heginbottom, J. A., & Melnikov, E. (2002). *Circum-arctic map of permafrost and ground-ice conditions, version 2.* National Snow and Ice Data Center. [Shapefile and metadata] Retrieved from https://nsidc.org/data/ggd318

Cajander, A. K. (1913). Studien über die Moore Finnlands [Study on the mires of Finland]. *Acta Forestalia Fennica*, *2*, 1–208. https://doi.org/10.14214/aff.7530

Carpino, O., Haynes, K., Connon, R., Craig, J., Devoie, É., & Quinton, W. (2021). Long-term climate-influenced land cover change in discontinuous permafrost peatland complexes. *Hydrology and Earth System Sciences*, *25*(6), 3301–3317. https://doi.org/10.5194/hess-25-3301-2021

Carpino, O. A., Berg, A., Quinton, W. L., & Adams, J. R. (2018). Climate change and permafrost thaw-induced boreal forest loss in northwestern. *Canada Environmental Research Letters*, *13*, 84018. https://doi.org/10.1088/1748-9326/aad74e

Chapin, A. F. S., Peterson, G., Berkes, F., Callaghan, T. V., Angelstam, P., Beier, C., Bergeron, Y., Crépin, A., Danell, K., Elmqvist, T., Folke, C., Forbes, B., Juday, G., Niemelä, J., Shvidenko, A., & Whiteman, G. (2004). Resilience and vulnerability of northern regions to social and environmental change. *Ambio*, *33*(6), 344–349. https://doi.org/10.1579/0044-7447-33.6.344

Chasmer, L., & Hopkinson, C. (2017). Threshold loss of discontinuous permafrost and landscape evolution. *Global Change Biology*, *23*(7), 2672–2686. https://doi.org/10.1111/gcb.13537

Chasmer, L., Hopkinson, C., & Quinton, W. (2010). Quantifying errors in discontinuous permafrost plateau change from optical data, Northwest Territories, Canada: 1947–2008. *Canadian Journal of Remote Sensing*, *36*, S211–S223. https://doi.org/10.5589/m10-058

Chasmer, L., Hopkinson, C., Veness, T., Quinton, W., & Baltzer, J. (2014). A decision-tree classification for low-lying complex land cover types within the zone of discontinuous permafrost. *Remote Sensing of Environment*, *143*, 73–84. https://doi.org/10.1016/j.rse.2013.12.016

Connon, R., Devoie, É., Hayashi, M., Veness, T., & Quinton, W. (2018). The influence of shallow taliks on permafrost thaw and active layer dynamics in subarctic Canada. *Journal of Geophysical Research - Earth Surface*, *123*(2), 281–297. https://doi.org/10.1002/2017JF004469

Connon, R. F., Quinton, W. L., Craig, J. R., Hanisch, J., & Sonnentag, O. (2015). The hydrology of interconnected bog complexes in discontinuous permafrost terrains. *Hydrological Processes*, *29*(18), 3831–3847. https://doi.org/10.1002/hyp.10604

Connon, R. F., Quinton, W. L., Craig, J. R., & Hayashi, M. (2014). Changing hydrologic connectivity due to permafrost thaw in the lower Liard River valley, NWT, Canada. *Hydrological Processes*, *28*, 4163–4178. https://doi.org/10.1002/hyp.10206

Devoie, É. G., & Craig, J. R. (2020). A semianalytical interface model of soil freeze/thaw and permafrost evolution. *Water Resources Research*, *56*(8), 1–16. https://doi.org/10.1029/2020WR027638

Devoie, É. G., Craig, J. R., Connon, R. F., & Quinton, W. L. (2019). Taliks: A tipping point in discontinuous permafrost degradation in peatlands.

Water Resources Research, *55*(11), 9838–9857. https://doi.org/10.1029/2018WR024488

Dingman, S. L. (2002). *Physical hydrology* (Second ed.). Waveland Press, Inc.

Environment and Climate Change Canada (ECCC). (2022). 1981–2010 Climate Normals & Averages. [Summary data tables] Retrieved from climate.weather.gc.ca.

ESRI. (2018–2021). *ArcGIS desktop: releases 10.5–10.7.* Environmental Systems Research Institute.

Freeze, R. A., & Cherry, J. A. (1979). *Groundwater.* Prentice-Hall, Inc.

Galkina, E. A. (1964). Metody ispol'zovaniya aerofotosnimkov dlya tipizatsii i kartirovaniya bolotnykh massivov [Methods of the use of air photos for typology and mapping of mire massifs]. In M. Ramenskaya (Ed.), Bolota i zabolochchennye zemli Karelii [Swamps and bogs of Keralia] (pp. 5–24). Karel'skoe izdatel'stvo.

Galkina, E. A., & Kiryushkin, V. (1969). Znachenie aerofotos'emki dlya ustanovleniya morfogeneticheskikh klassifikatsii bolonykh urochishch i sistem [Importance of aerophotography for the morpho-genetic classification of bog massifs and systems]. In Doklady komissi aerofotos'emki i fotogrammetrii [Reports of the commission of aerial photography and photogrammetry] (Vol. 6). Geograficheskoe obshchestvo.

Gibson, C., Cottenie, K., Gingras-Hill, T., Kokelj, S. V., Baltzer, J. L., Chasmer, L., & Turetsky, M. R. (2021). Mapping and understanding the vulnerability of northern peatlands to permafrost thaw at scales relevant to community adaptation planning. *Environmental Research Letters*, *16*(5), 055022. https://doi.org/10.1088/1748-9326/abe74b

Gorelick, N., Hancher, M., Dixon, M., Ilyushchenko, S., Thau, D., & Moore, R. (2017). Google Earth Engine: Planetary-scale geospatial analysis for everyone. *Remote Sensing of Environment*, *202*, 18–27. https://doi.org/10.1016/j.rse.2017.06.031

Harris, S. A., French, H. M., Heginbottom, J. A., Johnston, G. B., Ladanyi, B., Sego, D. C., & van Everdingen, R. O. (1988). Glossary of permafrost and related ground-ice terms. In *The permafrost environment.* National Research Council of Canada. https://doi.org/10.1139/t88-045

Hayashi, M., Quinton, W. L., Pietroniro, A., & Gibson, J. J. (2004). Hydrologic functions of wetlands in a discontinuous permafrost basin indicated by isotopic and chemical signatures. *Journal of Hydrology*, *296*, 81–97. https://doi.org/10.1016/j.jhydrol.2004.03.020

Haynes, K. M., Connon, R. F., & Quinton, W. L. (2018). Permafrost thaw induced drying of wetlands at Scotty Creek, NWT. *Environmental Research Letters*, *13*(11), 114001. https://doi.org/10.1088/1748-9326/aae46c

Henton, J., Craymer, M. R., Ferland, R., Dragert, H., & Forbes, D. (2006). Crustal motion and deformation monitoring of the Canadian landmass. *Geomatica*, *60*(2), 173–191.

Hopkinson, C., Wulder, M. A., Coops, N. C., Milne, T., Fox, A., & Bater, C. W. (2011). Airborne lidar sampling of the Canadian boreal forest: Planning, execution & initial processing. Proceedings of the SilviLaser 2011 Conference, Oct. 16-20. 2011:unpaginated USB.

Ivanov, K. (1975). Vodoobmen v bolotnykh landshaftakh [Water movement in mirelands]. Gidrometeoizdat.

Kirkham, M. B. (2005). Electrical analogues for water movement through the soil-plant-atmosphere continuum. In *Principles of soil and plant water relationships* (pp. 341–356). Elsevier Inc. https://doi.org/10.1016/B978-012409751-3/50020-7

Kirkwood, A., Roy-Leveillee, P., Packalen, M. S., Mclaughlin, J., & Basiliko, N. (2019). Evolution of palsas and peat plateaus in the Hudson Bay Lowlands: Permafrost degradation and the production of greenhouse gases. In J. Bilodeau, D. F. Nadeau, D. Fortier, & D. Conciatori (Eds.), *18th International Conference on Cold Regions Engineering and the 8th Canadian Permafrost Conference (ICCRE/CPC)* (pp. 597–606). American Society of Civil Engineers.

Kirpotin, S. N., Polishchuk, Y., & Bryksina, N. (2009). Abrupt changes of thermokarst lakes in Western Siberia: Impacts of climatic warming on

permafrost melting. *International Journal of Environmental Studies*, *66*(4), 423–431. https://doi.org/10.1080/00207230902758287

Kuhry, P. (2008). Palsa and peat plateau development in the Hudson Bay Lowlands, Canada: Timing, pathways, and causes. *Boreas*, *37*(2), 316–327. https://doi.org/10.1111/j.1502-3885.2007.00022.x

Kværner, J., & Kløve, B. (2008). Generation and regulation of summer runoff in a boreal flat fen. *Journal of Hydrology*, *360*, 15–30. https://doi.org/10.1016/j.jhydrol.2008.07.009

Luoto, M., & Seppälä, M. (2002). Modelling the distribution of palsas in Finnish Lapland with logistic regression and GIS. *Permafrost and Periglacial Processes*, *13*, 17–28. https://doi.org/10.1002/ppp.404

Luoto, M., & Seppälä, M. (2003). Thermokarst ponds as indicators of the former distribution of palsas in Finnish Lapland. *Permafrost and Periglacial Processes*, *14*(1), 19–27. https://doi.org/10.1002/ppp.441

Mack, M., Connon, R., Makarieva, O., McLaughlin, J., Nesterova, N., & Quinton, W. (2021). Heterogenous runoff trends in peatland-dominated basins throughout the circumpolar north. *Environmental Research Communications*, *3*(7), 75006. https://doi.org/10.1088/2515-7620/ac11ed

McCarter, C. P. R., & Price, J. S. (2017). Experimental hydrological forcing to illustrate water flow processes of a subarctic ladder fen peatland. *Hydrological Processes*, *31*, 1578–1589. https://doi.org/10.1002/hyp.11127

McLaughlin, J., & Webster, K. (2014). Effects of climate change on peatlands in the far north of Ontario, Canada: A synthesis. *Arctic, Antarctic, and Alpine Research*, *46*(1), 84–102. https://doi.org/10.1657/1938-4246-46.1.84

Milne, T., Monette, S., Luther, J., Fournier, R., Hopkinson, C. & Bowers, W. (2012). Lidar Processing Software In Support Of The Newfoundland Fibre Inventory Project. Proceedings of the 33rd Canadian Symposium on Remote Sensing, Ottawa, Ontario, Canada June 11–14. Unpaginated

National Oceanic and Atmospheric Administration (NOAA). (2022). Climate at a Glance Global Time Series [CSV annual temperature anomalies for 53 °N, 86 °W] Retrieved from https://www.ncei.noaa.gov/access/monitoring/climate-at-a-glance/global/time-series

National Wetlands Working Group (NWWG). (1988). *Wetlands of Canada*. Polyscience Publications, Inc.

National Air Photo Library (NAPL). (2018). Natural Resources Canada. [Digitalised air photographs] Retrieved from www.nrcan.gc.ca

National Fire Database (NFDB). (2022). Natural Resources Canada. National Burned Area Composite [Vector GIS dataset] Retrieved from https://cwfis.cfs.nrcan.gc.ca/datamart/metadata/nbac

Ontario Ministry of Natural Resources and Forestry (OMNRF). (2014). Far North Land Cover: Data Specifications Version 1.4. [Shapefile and supporting document] Retrieved from https://geohub.lio.gov.on.ca

Ou, C., LaRocque, A., Leblon, B., Zhang, Y., Webster, K., & McLaughlin, J. (2016). Modelling and mapping permafrost at high spatial resolution using Landsat and Radarsat-2 images in Northern Ontario, Canada: Part 2—Regional mapping. *International Journal of Remote Sensing*, *37*(12), 2751–2779. https://doi.org/10.1080/01431161.2016.1151574

Packalen, M., Finkelstein, S., & McLaughlin, J. (2014). Carbon storage and potential methane productions in the Hudson Bay Lowlands since mid-Holocene peat initiation. *Nature Communications*, *5*, 4078. https://doi.org/10.1038/ncomms5078

Pala, S., Barnett, P., & Babuin, D. (1991). Quaternary geology of Ontario, northern sheet [shapefile and metadata]. Map 2553, Ontario Geological Survey. Retrieved from https://www.geologyontario.mndm.gov.on.ca/ogsearth.html

Payette, S., Delwaide, A., Caccianiga, M., & Beauchemin, M. (2004). Accelerated thawing of subarctic peatland permafrost over the last 50 years. *Geophysical Research Letters*, *31*(18), 1, L18208–4. https://doi.org/10.1029/2004GL020358

Pironkova, Z. (2017). Mapping palsa and peat plateau changes in the Hudson Bay Lowlands, Canada, using historical aerial photography and high-resolution satellite imagery. *Canadian Journal of Remote Sensing*, *43*(5), 455–467. https://doi.org/10.1080/07038992.2017.1370366

Price, J. S. (1987). The influence of wetland and mineral terrain types on snowmelt runoff in the subarctic. *Canadian Water Resources Journal*, *12*(2), 43–52. https://doi.org/10.4296/cwrj1202043

Price, J. S., & Maloney, D. A. (1994). Hydrology of a patterned bog-fen complex in southeastern Labrador, Canada. *Nordic Hydrology*, *25*, 313–330. https://doi.org/10.2166/nh.1994.0011

Quinton, W. L., & Baltzer, J. L. (2013). The active-layer hydrology of a peat plateau with thawing permafrost (Scotty Creek, Canada). *Hydrogeology Journal*, *21*, 201–220. https://doi.org/10.1007/s10040-012-0935-2

Quinton, W. L., Elliot, T., Price, J. S., Rezanezhad, F., & Heck, R. (2009). Measuring physical and hydraulic properties of peat from X-ray tomography. *Geoderma*, *153*(1–2), 269–277. https://doi.org/10.1016/j.geoderma.2009.08.010

Quinton, W. L., Hayashi, M., & Pietroniro, A. (2003). Connectivity and storage functions of channel fens and flat bogs in northern basins. *Hydrological Processes*, *17*(18), 3665–3684. https://doi.org/10.1002/hyp.1369

Quinton, W. L., & Roulet, N. T. (1998). Spring and summer runoff hydrology of a subarctic patterned wetland. *Arctic and Alpine Research*, *30*(3), 285–294. https://doi.org/10.2307/1551976

R Core Team. (2022). *R: A language and environment for statistical computing*. R Foundation for Statistical Computing. http://r-project.org/

Radforth, N. W. (1969). Classification of muskeg. In *Muskeg engineering handbook* (pp. 31–52). University of Toronto Press.

Rezanezhad, F., Price, J. S., Quinton, W. L., Lennartz, B., Milojevic, T., & Van Cappellen, P. (2016). Structure of peat soils and implications for water storage, flow and solute transport: A review update for geochemists. *Chemical Geology*, *429*, 75–84. https://doi.org/10.1016/j.chemgeo.2016.03.010

Richardson, M., Ketcheson, S., Whittington, P., & Price, J. (2012). The influences of catchment geomorphology and scale on runoff generation in a northern peatland complex. *Hydrological Processes*, *26*, 1805–1817. https://doi.org/10.1002/hyp.9322

Riley, J. L. (2011). *Wetlands of the Ontario Hudson Lowland: A regional overview*. Nature Conservancy of Canada.

Roulet, N. T., & Woo, M. K. (1988). Runoff generation in a low Arctic drainage basin. *Journal of Hydrology*, *101*(1–4), 213–226. https://doi.org/10.1016/0022-1694(88)90036-4

Rouse, W. R. (1998). A water balance model for a subarctic sedge fen and its application to climatic change. *Climatic Change*, *38*(2), 207–234. https://doi.org/10.1023/A:1005358017894

Sjörs, H. (1959). Bogs and fens in the Hudson Bay Lowlands. *Arctic*, *12*(1), 2–19. https://doi.org/10.14430/arctic3709

Spence, C., Norris, M., Bickerton, G., Bonsal, B. R., Brua, R., Culp, J. M., Dibike, Y., Gruber, S., Morse, P. D., Peters, D. L., Shrestha, R., & Wolfe, S. A. (2020). The Canadian water resource vulnerability index to permafrost thaw (CWRVI$_{PT}$). *Arctic Science*, *6*(4), 437–462. https://doi.org/10.1139/as-2019-0028

Spence, C., & Woo, M. K. (2003). Hydrology of subarctic Canadian shield: Soil-filled valleys. *Journal of Hydrology*, *279*(1–4), 151–166. https://doi.org/10.1016/S0022-1694(03)00175-6

Spence, C., & Woo, M. K. (2006). Hydrology of subarctic Canadian shield: Heterogeneous headwater basins. *Journal of Hydrology*, *317*(1–2), 138–154. https://doi.org/10.1016/j.jhydrol.2005.05.014

St. Jacques, J. S., & Sauchyn, D. J. (2009). Increasing winter baseflow and mean annual streamflow from possible permafrost thawing in the Northwest Territories, Canada. *Geophysical Research Letters*, *36*, L01401. https://doi.org/10.1029/2008GL035822

Vallée, S., & Payette, S. (2007). Collapse of permafrost mounds along a subarctic river over the last 100 years (northern Québec).

Geomorphology, *90*(1–2), 162–170. https://doi.org/10.1016/j.geomorph.2007.01.019

Vitt, D. H., Halsey, L. A., & Zoltai, S. C. (1994). The bog landforms of continental western Canada in relation to climate and permafrost patterns. *Permafrost and Periglacial Processes*, *26*(1), 1–13. https://doi.org/10.1111/j.1502-3885.2007.00022.x

Waddington, J. M., Kellner, E., Strack, M., & Price, J. S. (2010). Differential peat deformation, compressibility, and water storage between peatland microforms: Implications for ecosystem function and development. *Water Resources Research*, *46*(7), 1–13. https://doi.org/10.1029/2009WR008802

Waddington, J. M., Morris, P. J., Kettridge, N., Granath, G., Thompson, D. K., & Moore, P. A. (2015). Hydrological feedbacks in northern peatlands. *Ecohydrology*, *8*, 113–127. https://doi.org/10.1002/eco.1493

Wright, N., Quinton, W. L., & Hayashi, M. (2008). Hillslope runoff from ice-cored peat plateaus in a discontinuous permafrost basin, Northwest Territories, Canada. *Hydrological Processes*, *22*, 2816–2828. https://doi.org/10.1002/hyp.7005

Wulder, M. A., White, J. C., Bater, C. W., Coops, N. C., Hopkinson, C., & Chen, G. (2012). Lidar plots a new large-area data collection option: Context, concepts, and case study. *Canadian Journal of Remote Sensing*, *38*(5), 1–19. https://doi.org/10.5589/m12-049

Zhang, Y., Lu, J., Wang, X., Chen, W., Sladen, W., Dyke, L., Dredge, L., Poitevin, J., McLennan, D., Stewart, H., Kowalchuk, S., Wu, W., Kershaw, G. P., & Brook, R. K. (2012). Modelling and mapping permafrost at high spatial resolution in Wapusk National Park, Hudson Bay Lowlands. *Canadian Journal of Earth Sciences*, *49*, 925–937. https://doi.org/10.1139/e2012-031

Zoltai, S. C., & Tarnocai, C. (1974). Perennially frozen peatlands in western arctic and subarctic of Canada. *Canadian Journal of Earth Sciences*, *12*, 28–43. https://doi.org/10.1139/e75-004

Zoltai, S. C., & Vitt, D. H. (1995). Canadian wetlands: Environmental gradients and classification. *Vegetatio*, *118*(1–2), 131–137. https://doi.org/10.1007/BF00045195

SUPPORTING INFORMATION

Additional supporting information can be found online in the Supporting Information section at the end of this article.